AD-A158 734 LASER PRODUCED X-RAY FOR HIGH RESOLUTION LITHOGRAPHY (U) BATTELLE COLUMBUS LABS OH H M EPSTEIN 17 APR 85 AFOSR-TR-85-0501 AFOSR-82-0066 1/1

UNCLASSIFIED F/G 14/5 NL

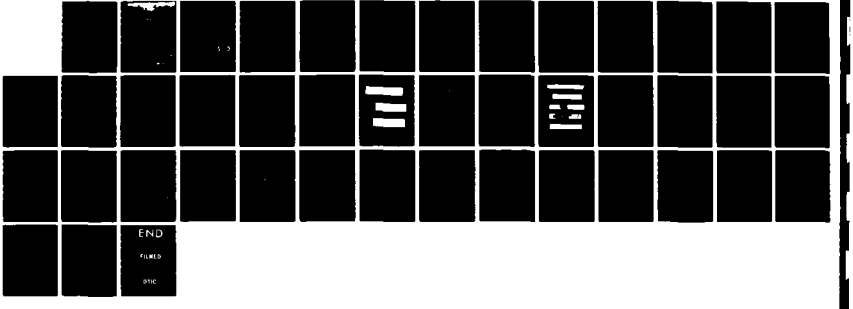

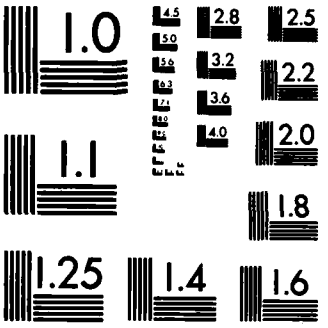

Report

LASER PRODUCED X-RAY FOR HIGH RESOLUTION LITHOGRAPHY

to

U.S. AIR FORCE
OFFICE OF SCIENTIFIC RESEARCH

April 17, 1985

Approved for public release;
distribution unlimited.

TOPICAL REPORT

on

LASER PRODUCED X-RAY FOR HIGH RESOLUTION LITHOGRAPHY

to

U.S. AIR FORCE
OFFICE OF SCIENTIFIC RESEARCH

April 17, 1985

by

Harold M. Epstein

BATTELLE
Columbus Laboratories
505 King Avenue
Columbus, Ohio 43201

UNCLASSIFIED
SECURITY CLASSIFICATION OF THIS PAGE

AD A 158 734

REPORT DOCUMENTATION PAGE

1a. REPORT SECURITY CLASSIFICATION Unclassified	1b. RESTRICTIVE MARKINGS
2a. SECURITY CLASSIFICATION AUTHORITY	3. DISTRIBUTION/AVAILABILITY OF REPORT Approved for public release; Distribution unlimited
2b. DECLASSIFICATION/DOWNGRADING SCHEDULE	
4. PERFORMING ORGANIZATION REPORT NUMBER(S)	5. MONITORING ORGANIZATION REPORT NUMBER(S) AFOSR-TR- 85-0501
6a. NAME OF PERFORMING ORGANIZATION Battelle 6b. OFFICE SYMBOL (If applicable)	7a. NAME OF MONITORING ORGANIZATION AFOSR/NP
6c. ADDRESS (City, State and ZIP Code) 505 King Avenue Columbus, OH 43201	7b. ADDRESS (City, State and ZIP Code) Building 410 Bolling AFB DC 20332-6448
8a. NAME OF FUNDING/SPONSORING ORGANIZATION AFOSR 8b. OFFICE SYMBOL (If applicable) NP	9. PROCUREMENT INSTRUMENT IDENTIFICATION NUMBER AFOSR 82-0066
8c. ADDRESS (City, State and ZIP Code) Building 410 Bolling AFB DC 20332-6448	10. SOURCE OF FUNDING NOS. PROGRAM ELEMENT NO. 61102F; PROJECT NO. 2301; TASK NO. A8; WORK UNIT NO.
11. TITLE (Include Security Classification) "LASER PRODUCED X-RAY FOR HIGH RESOLUTION LITHOGRAPHY"	
12. PERSONAL AUTHOR(S) Dr. Harold M. Epstein	
13a. TYPE OF REPORT ANNUAL 13b. TIME COVERED FROM 15 Dec 83 TO 14 Dec 84	14. DATE OF REPORT (Yr., Mo., Day) April 17, 1985 15. PAGE COUNT 39
16. SUPPLEMENTARY NOTATION	
17. COSATI CODES FIELD / GROUP / SUB. GR.	18. SUBJECT TERMS (Continue on reverse if necessary and identify by block number)

19. ABSTRACT (Continue on reverse if necessary and identify by block number)

During the past year the research effort was concentrated on the rapidly pulsed laser-plasma x-ray source. The effort was divided into three areas: developing the source and system, studying improved diagnostics, and making accurate x-ray measurements over a parameter matrix.

20. DISTRIBUTION/AVAILABILITY OF ABSTRACT UNCLASSIFIED/UNLIMITED ☒ SAME AS RPT. ☐ DTIC USERS ☐	21. ABSTRACT SECURITY CLASSIFICATION Unclasified
22a. NAME OF RESPONSIBLE INDIVIDUAL Dr Robert J. Barker	22b. TELEPHONE NUMBER (Include Area Code) 202/767-5011 22c. OFFICE SYMBOL NP

DD FORM 1473, 83 APR EDITION OF 1 JAN 73 IS OBSOLETE.

UNCLASSIFIED
SECURITY CLASSIFICATION OF THIS PAGE

TABLE OF CONTENTS

LIST OF TABLES

LIST OF FIGURES

LASER PRODUCED X-RAY FOR HIGH RESOLUTION LITHOGRAPHY

by

Harold M. Epstein

INTRODUCTION

It is well established that x-ray lithography is an effective means for replicating submicrometer linewidth patterns.[1] Besides replicating test patterns, the technique has been used to fabricate surface acoustic wave devices, bubble domain devices, pn diodes, bipolar transistors, and MOS transistors. The basic concept of x-ray lithography is to use the short wavelength of an x-ray source instead of the long wavelength of an ultraviolet source. This essentially eliminates the diffraction limitation of the ultraviolet source. With this eliminated, x-ray lithography is capable of producing line patterns with a "line width accuracy" of less than 0.1 μm.

The laser-plasma x-ray source has developed into the most intense laboratory x-ray source available in the energy range of ∿ 3/4 to 2 keV. In addition, it appears to be the most attractive laboratory high-average-power x-ray source in the energy range. This energy range is particularly significant for microlithography of integrated circuits. There can be little doubt about the need for high intensity and high-average-power x-ray sources which operate in this energy range, and which are small enough to be used in a laboratory or industrial locations. The rapid growth of synchroton x-ray facilities demonstrates the increasing importance of high-average-power soft x-ray sources. However, the synchrotron is excluded as a laboratory x-ray source because of its size and cost. The commercial applications should expand greatly when the source becomes readily available at the home facility of the user.

In this report the basic phenomenology of the laser plasma x-ray source is studied over an extended range with a rapidly pulsed mode-locked laser system. The use of this quasi-steady state source permitted extensive evaluation of a variety of parameters which have not been studied in detail before. These include the preparation of the initial plasma profile, the main pulse width, and the pulse amplitude. The parameter ranges bridged the regime between steady-state and nonsteady-state models.

References are located on Page 37.

To evaluate the plasma phenomonology, it was necessary to investigate several diagnostic techniques not commonly used on laser plasmas. These include rise time scintillator pulse shape analyzers and fast decay component measurements. Also, steady-state calorimetry, spectroscopy, and pin-hole photography were possible because of the quasi-steady-state nature of the source.

Because the high repetition rate laser-plasma x-ray source is a new concept, a large portion of the program was necessarily devoted to developing the technique, troubleshooting problems, and optimizing the source. These included optimizing the rotation rate of the target; devising systems to prevent the lens from being destroyed by focused reflections when a small amount of target blowoff negated the antireflection coating on one side of the lens; and maintaining consistent output from the mode locked laser. One of the main conclusions of this study is that these problems can be overcome and that this type of soft x-ray source is very valuable for research and ultimately for commercial lithography.

RESULT OF RESEARCH DURING THIS PERIOD

During the past year the research effort was concentrated on the rapidly pulsed laser-plasma x-ray source. The effort was divided into three areas: developing the source and system, studying improved diagnostics, and making accurate x-ray measurements over a parameter matrix.

Source Development

In previous studies, efficient x-ray generation with small mode locked laser pulses, capable of irradiating targets at $\sim 10^{14}$ w/cm^2, was established with single pulse tests. At the end of the previous program, a limited number of quasi-steady-state tests were run with 30 psec pulses of approximately 50 mj. The rotation speed of the target was very high to assure a very clean surface for each pulse. The total number of pulses in a test was small enough that metal plating on the lens and detector windows was negligible.

The laser targets which comprised the x-ray source were 2.5 cm diameter by 2.0 cm long, yielding an area of 15.2 cm^2. Since the laser focal spot size can be less than 50 μm, over one half million pulses might be obtained from a single target. Actually the screw drive in our system was a standard micrometer with about 625 μm advance per turn. This limits the possible target life to approximately 50,000 pulses. As shown in Figure 1, the x-ray yield does not decrease significantly until the spacing between pulses is less than about 70 μm. On the order of 50,000 pulses per target can be obtained from the present system, and this can be extended to about 500,000 pulses with a finer screw drive. The life of the target can easily be extended to equal the life of the laser flash lamps by using bigger cylinders. The flash lamps of the Quantel laser employed for the present experiment have a rated life of approximately 1,000,000 flashes.

The second problem associated with a repetitively pulsed laser is that the vaporized target material eventually builds up a thin reflecting coating on the lens, which defeats the antireflection coating. This deposited layer is thin enough that the energy loss is essentially negligible for one target lifetime. However, the small amount of reflected light can be multiply reflected to a focus in the lens, causing progressive damage. This problem was solved by expanding the beam by about a factor of five and using a lens with an equivalent f number but a factor of five further away. A hole was drilled in the center of the lens to eliminate multiple reflective focusing at the center. Since brightness is conserved in this change, the size of the focal spot is the same, and the x-ray generation is unaffected.

Diagnostic Techniques

The principal diagnostic techniques are crystal diffraction spectroscopy, steady-state calorimetry, and pulse width measurements. Spectra were taken with a flat KAP crystal. Since the quasi-steady-state spectroscopy differed from the single pulse experiments only in the photon statistics, no further discussion of this technique is needed.

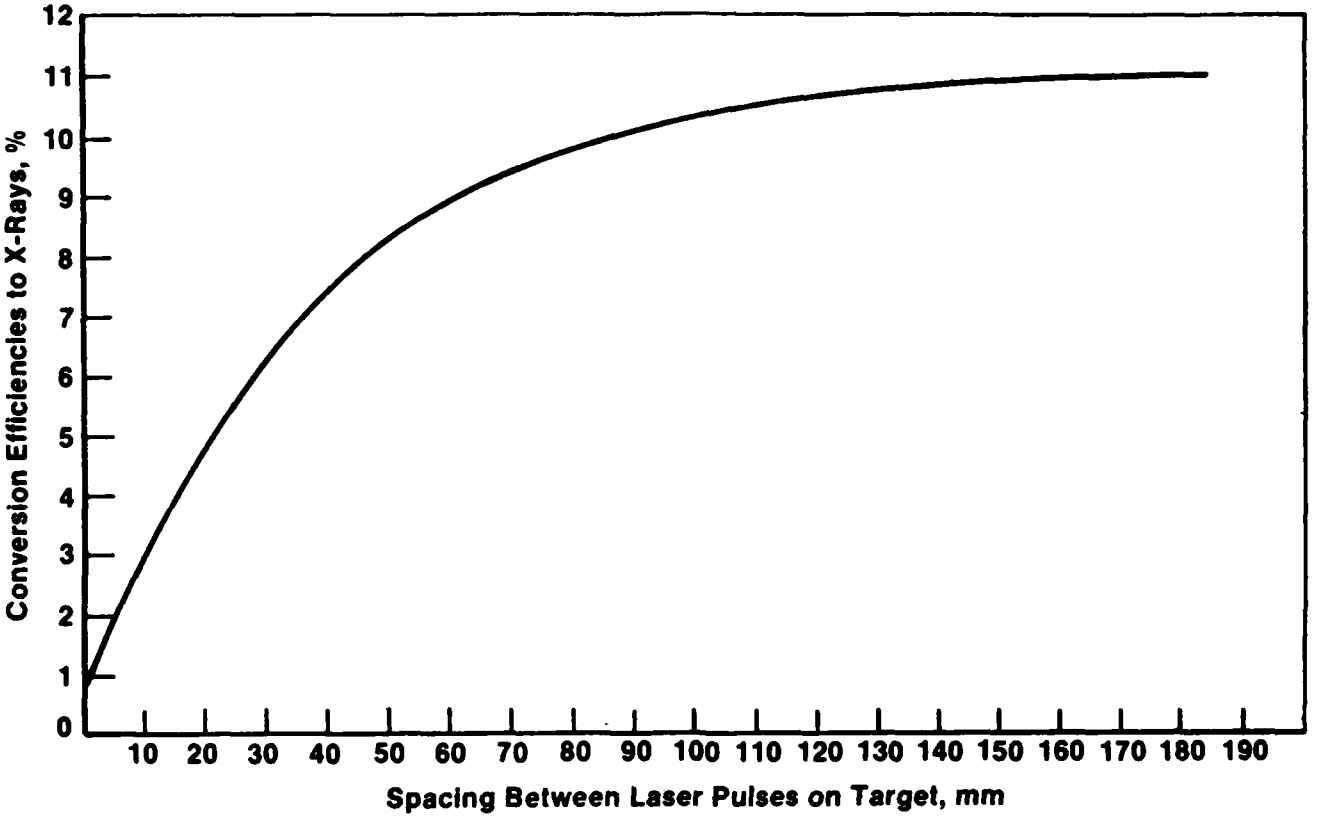

FIGURE 1. EFFECT OF FOCAL SPOT SPACING ON X-RAY CONVERSION EFFICIENCY

Single pulse x-ray calorimetry is usually done with pyroelectric detectors. These have some inherent uncertainties in this type of application because of the sensitivity of this type of detector to mechanical vibrations or small shocks. The pure calorimetric detector applicable to the quasi-steady state or high repetition rate experiments is inherently more accurate and more stable. The principle precaution that must be taken with the steady state calorimeter is to make certain that the debris heat doesn't register in the calorimeter.

Two distinct experimental techniques were compared in the time dependent diagnostics of the x-ray pulse. Both methods have a time resolution capability limited by the detector to 9×10^{-11} seconds. The detector was a Hamamatsu photodiode. The first method is based on the fast rise time characteristics of unitary crystals. If a scintillator could be found with a perfectly sharp rise and a very long decay time, the pulse shape of the emitted light would simply represent the time integrated x-ray flux, and a time resolved pulse would be obtained by differentiating the corrected intensity profile. In practice, the fast rise is attainable, but the long decay is elusive. The rise time of organic crystals in general is a function of the concentration of the fluorescent solute.[2] Since time is required for energy deposited in the solvent to diffuse to active solute, the major emitted component of the binary or tertiary, liquid or plastic scintillator should have a rise time too long for subnanosecond resoltuion. Of course, a small component of the x-ray energy will be deposited directly in the solute, producing a weak signal of very fast rise time. The use of this signal will be discussed in the second method.

In any case a logical alternative to the binary or tertiary detector is to use a unitary fluorescent material. The rise time is limited only by the equilibration time of the incident x-ray energy for unitary organic crystals such as anthracene or stilbene. This time is of the order of picoseconds for the low energy x-rays of interest here. The x-rays are absorbed by the photoelectric effect and the emitted electrons slow down in about 10^{-12} seconds raising the molecules of the scintillator to upper

level excited electronic states. These states decay in about 10^{-12} seconds by internal conversion, primarily to the lowest excited singlet state($^1X^*$), which decays by radiative emission producing the fast component of the visible scintillator output.[3] A slower component of the scintillator emission arises from the excited triplet state ($^3X^*$). The delayed emission is due to bimolecular association of $^3X^*$

$$^3X^* + {}^3X^* \rightarrow {}^1X^* + {}^1X$$

The decay rate of this slow component is not exponential and is dependent on the density of excitation.[4] Thus, a strongly ionizing charged heavy particle will exhibit a different decay time in the slow component than an x-ray or an electron, giving rise to the decay time discrimination technique often used to distinguish neutrons from gammas. This slow (typically 30 nanoseconds) component is erroneously quoted in handbooks as the fluorescent decay time of anthracene. However, in the subnanosecond regime, the contribution of the slow component to the scintillator output is unimportant and the fast component dominates. The time constant of the fast component is 1 nanosecond.

A 1-nanosecond decay time constant is hardly long, in the present experiments, but a correction for the decay can easily be applied to the differentiated curve, so that this is not a serious drawback to the technique. The light emission, E(t), from the scintillator at time,t, caused by the time-dependent x-ray fluence, S(t), is

$$E(t) = C\int_0^t dt'\, S(t')\, \exp-(t-t')/\tau \quad , \tag{1}$$

where τ is the decay time of the scintillator. Differentiating Equation (1) gives

$$d/dt[E(t)] = C\left[S(t) - \frac{1}{\tau}\int_0^t dt' S(t')\, \exp-(t-t')/\tau\right] \quad , \tag{2}$$

and substituting Equation (1) into (2),

$$S(t) = 1/C\ \{d/dt[E(t)] + E(t)/\tau\} \quad . \tag{3}$$

Equation (3) shows that a finite decay constant simply requires the addition of $E(t)/\tau$ to the derivative. It would certainly be preferable if a fast rise time scintillator were available with a longer decay time. However, the short decay constant and high scintillation efficiency of anthracene are advantageous where low x-ray intensities limit the accuracy of the measurements.

The second method for time dependent diagnostics is based on a characteristic of plastic scintillation observed by M. Dugay[5]. As mentioned earlier a fraction of the soft x-ray radiation in an organic scintillator is absorbed directly by the fluorescent solute, producing a very fast rise time component. Dugay observed that there is also a very fast time decay component in plastic scintillators. It is, therefore, possible to measure shapes of pulses which are short compared to the several nanosecond dominant time constant.

The x-rays passed through a 1/2 mil Be filter before entering the scintillator. The Be filter blocked out the laser pulse and the plasma light. The scintillor emissions were transmitted through a light pipe and into the photo diode after passing through an interference filter designed to remove any 1.06 μm laser light which might have leaked through pin holes in the Be. The x-ray output is almost the same as the laser pulse shape as shown in Figure 2.

Experimental Program

The experimental program primarily involved x-ray measurements over an extensive parameter matrix. The diagnostic methods discussed in the previous section along with those methods applied in previous years of this program were applied to a wide range of laser plasma conditions. Specifically, the parameters varied in this study were (1) laser pulse energy, (2) laser pulse width, (3) plasma profile, (4) laser wavelength, (5) target atomic number, (6) initial focal area, and (7) focal ratio of the lens. The laser pulse energy was varied from 0 to .3j, although the upper limit of the pulse energy was not available for the shortest pulse widths. Three laser pulse widths were used, 300 psec, 180 psec, and 30 psec. The majority

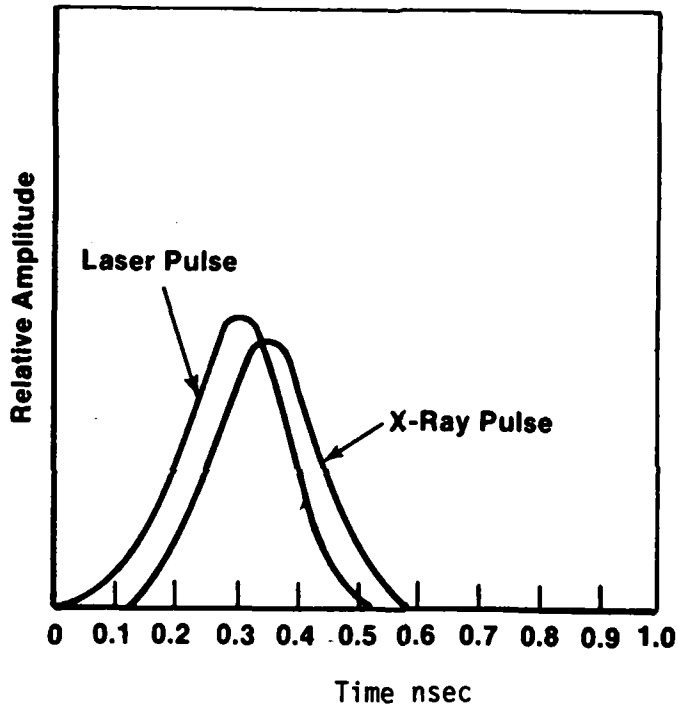

FIGURE 2. COMPARISON OF LASER PULSE WITH X-RAY PULSE

of the study was done at a wavelength of 1.06 μm. However, a limited study at 0.53 μm was completed. The plasma profile was modified over a wide range by varying the leakage foot through the pulse selector pockels cell. A wide variety of targets including Cu, Fe, Cr, Ti, V, Nb, Al, Mg, F, and W were included, but the majority of the parameter studies were done with Cu and Al. Only two lens focal ratios were employed.

Figure 3 shows the x-ray output efficiency over 1 keV for the 300, 180, and 30 psec pulses. From previous studies, we have shown that x-ray production efficiency reaches a maximum when the laser power is given by

$$P_L \approx 10^{14} \pi v \tau D_B \Delta \qquad (4)$$

where v is the average velocity of the expanding critical density front. For copper this is about 10^7 cm/sec. If the laser were diffraction limited, the beam divergence Δ would be $1.2\lambda/D_B$, where D_B is the beam diameter. Due to pumping stress induced distortions, the value of $D_B\Delta$ is 10^{-3} instead of 10^{-4}. For the .3 nsec pulse width, τ, the required laser pulse energy for efficient x-ray production is 0.6j. Only 0.3 *j/pulse* was available and losses in the optics decreased this by about 10 percent. As can be seen from Figure 3, the x-ray conversion efficiency for the 0.3 nsec pulse width is very low, and the efficiency drops off rapidly with decreasing energy for the .18 nsec pulse width below the value specified by Equation 4. As expected, considerably higher powers do not produce greater x-ray conversion efficiencies.

As long as the laser power is safely above the level specified by Equation 4, the x-ray conversion efficiency is essentially independent of pulse width until it begins to fall off at the shortest pulse widths of ~30 psec. The loss of efficiency at the shortest pulse width is probably due to the fact that the residency time of the ions in the heated region of the plasma is not sufficient to allow the ionization to approach steady state.

The effect of a low level of laser energy on the target before the main pulse is to prepare a plasma profile. This is accomplished by

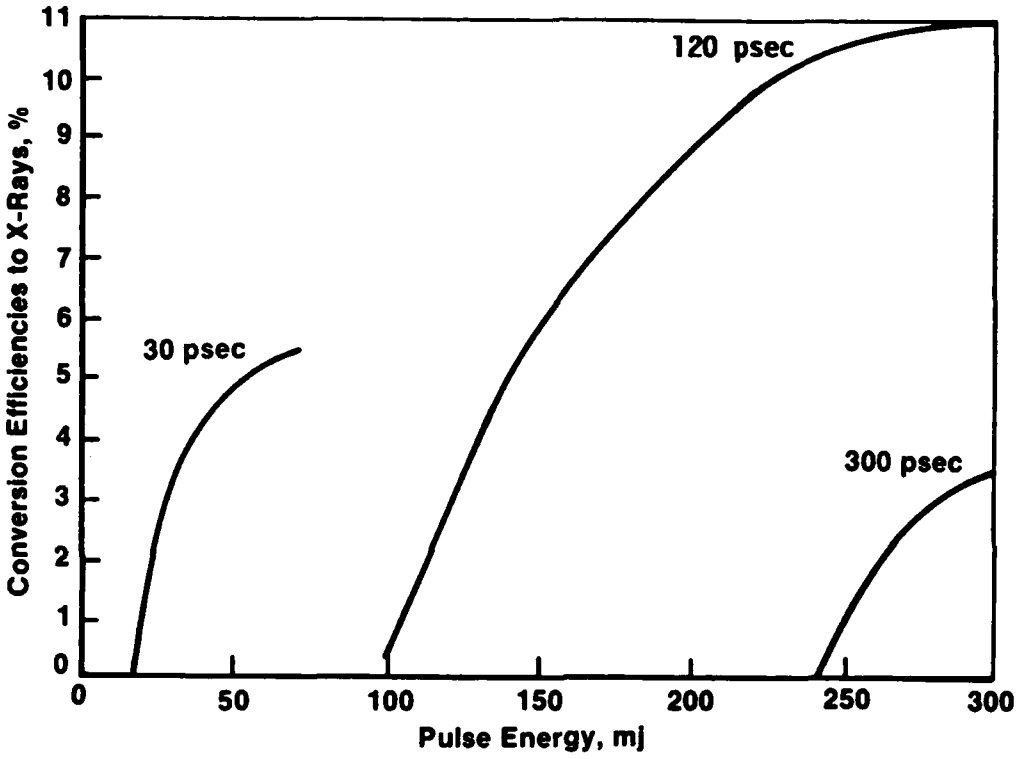

FIGURE 3. OUTPUT EFFICIENCY FOR X-RAYS OVER 1 keV

slightly opening the pockels cell on the pulse slicer. The calculated characteristic of this plasma foot are shown in the following equations:

$$T_\infty \approx \sigma^{-1/4} I_f^{1/4} \tag{5}$$

$$d \approx \left[\frac{(Z_\infty + 1)K}{M}\right]^{1/2} \sigma^{-1/8} I_f^{1/8} \tau_f \tag{6}$$

$$(n_i)_a \approx \frac{M^{1/2} \sigma^{3/8} I_f^{5/8}}{6(Z_\infty + 1)^{3/2} k^{3/2}} \tag{7}$$

where I_f is the foot intensity, σ is the Stefan-Boltzman constant, M is the ion mass, T_∞, Z^*_∞ are the assymptotic values of the temperature and mean ion effective charge respectively, τ_f is the pulse width of the laser foot, d is the foot-plasma thickness, and k is the Boltzman constant.

Although the leakage pulse has a series of mode locked spikes, the effective profile can be estimated by averaging over the spikes. As can be seen from Figure 4 the conversion efficiency is relatively insensitive to the amount of leakage foot over a very wide range for the more energetic main pulse. However, as the energy of the main pulse decreases, the effect of the foot becomes much more critical. this study was done only for the .18 nsec pulse width.

In addition to the experiments at 1.06 μm, a limited number of experiments were also conducted with a frequency doubled beam at 0.53 μm. The effect of laser foot on efficiency was the same for 0.53 μm as for 1.06 within the experimental accuracy. The x-ray spectrum and conversion efficiencies for the L-line x-rays are also the same for these two wavelengths. The k-line x-rays differ substantially for the 0.53 μm wavelength compared to the 1.06 μm. These differences are discussed under previous research results.

A variety of elements in the K and L-line emission regimes were investigated. The low atomic number elements were of particular interest because their spectra are required for the design of the x-ray pumped photoemission x-ray laser experiments planned for 1985. These elements include Al, Mg, Na, F, and C. Spectra for some of these elements are shown

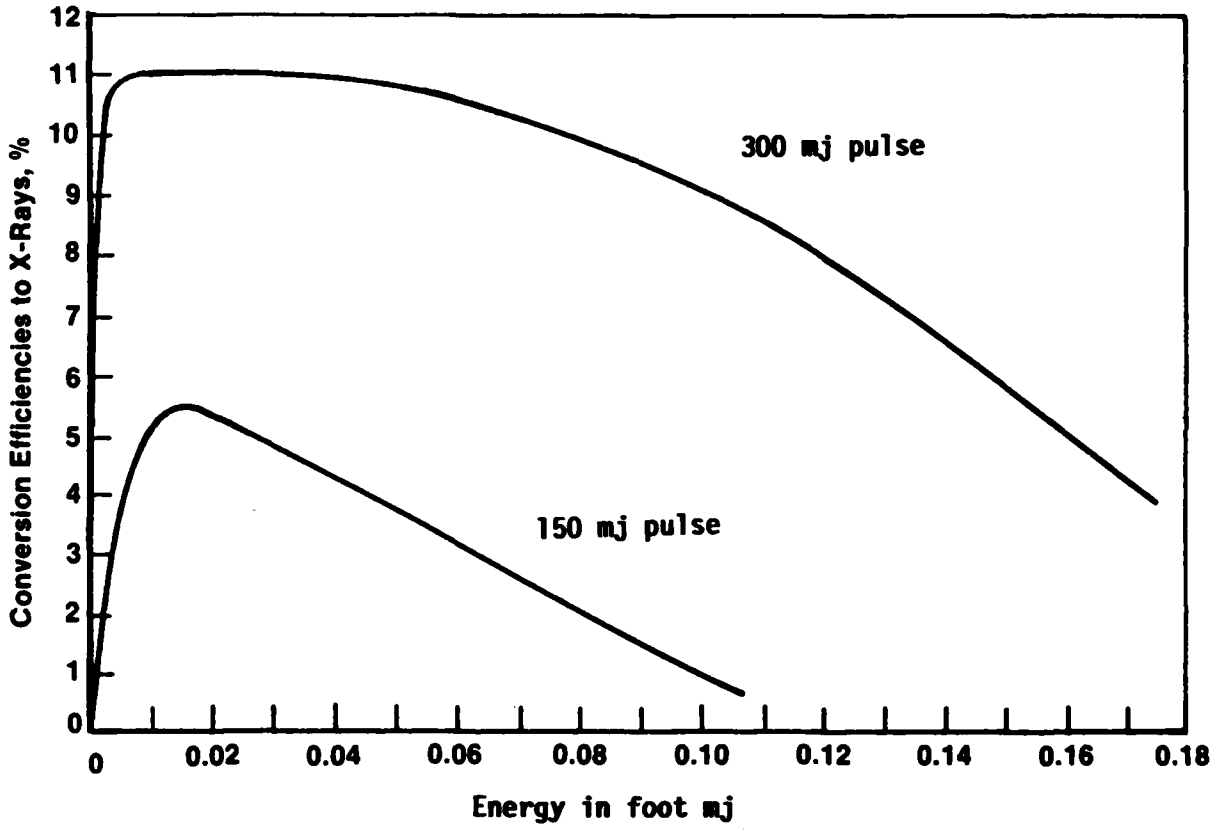

FIGURE 4. EFFECT OF PREPULSE ON X-RAY EFFICIENCY

in Figure 5. For Al and Mg the He-like resonance lines dominate, while for the lower atomic number element, such as F, the H-like lines dominate. This effect is shown in Figures 6 and 11.

The absorption of the emitted x-rays by the plasma is also of interest for computer modeling. Table 1 shows the ratio of the intensity of a number of lines measured near tangential to the target surface to the intensity of the same lines measured normal to the surface. Self-absorption of the line within the plasma gives a ratio less than one. Amplification, as with an x-ray laser, would give a ratio greater than one. As can be seen from Table 1, the line ratios are approximately 1 within experimental error. A second method to experimentally evaluate self absorption is to examine line profiles for self absorption dips in the center of the line. The absorption line width will be narrower than the emission width because Stark and Doppler broadening are lower in the colder less dense regions of the plasma. If stimulated absorption occurs, the absorption will be intensity dependent and the absorption line width will narrow during transport through the plasma.

TABLE 1. RATIO OF TANGENTIAL TO NORMAL INTENSITIES

Line						AL	
	1	2	3	4	5	6	8
R	1.05	1.02	.96	.94	.98	1.08	.94
Line						F	
R	.99	1.04	1.00	.95	.97	.94	1.03

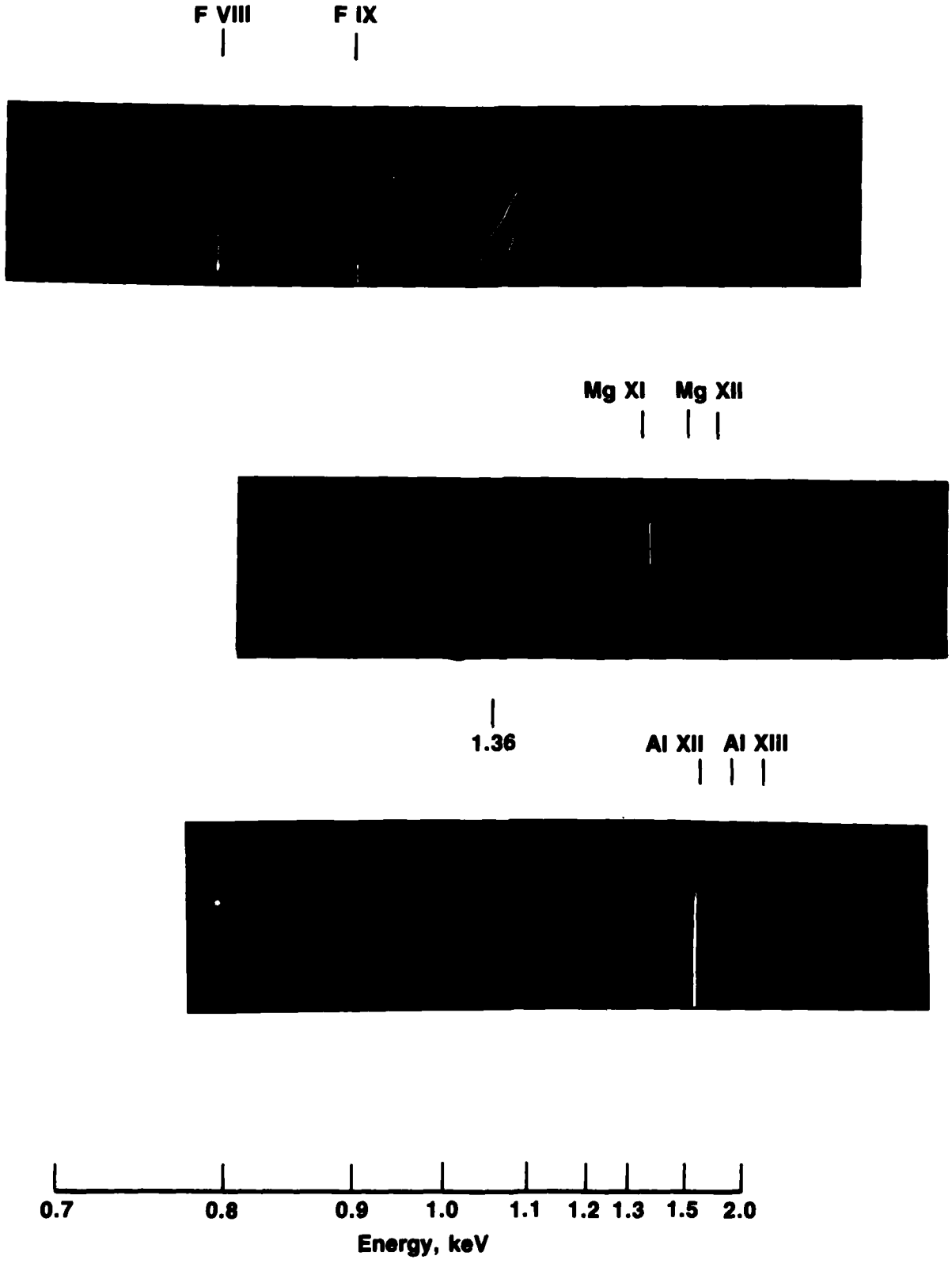

FIGURE 5. K-LINE SPECTRA

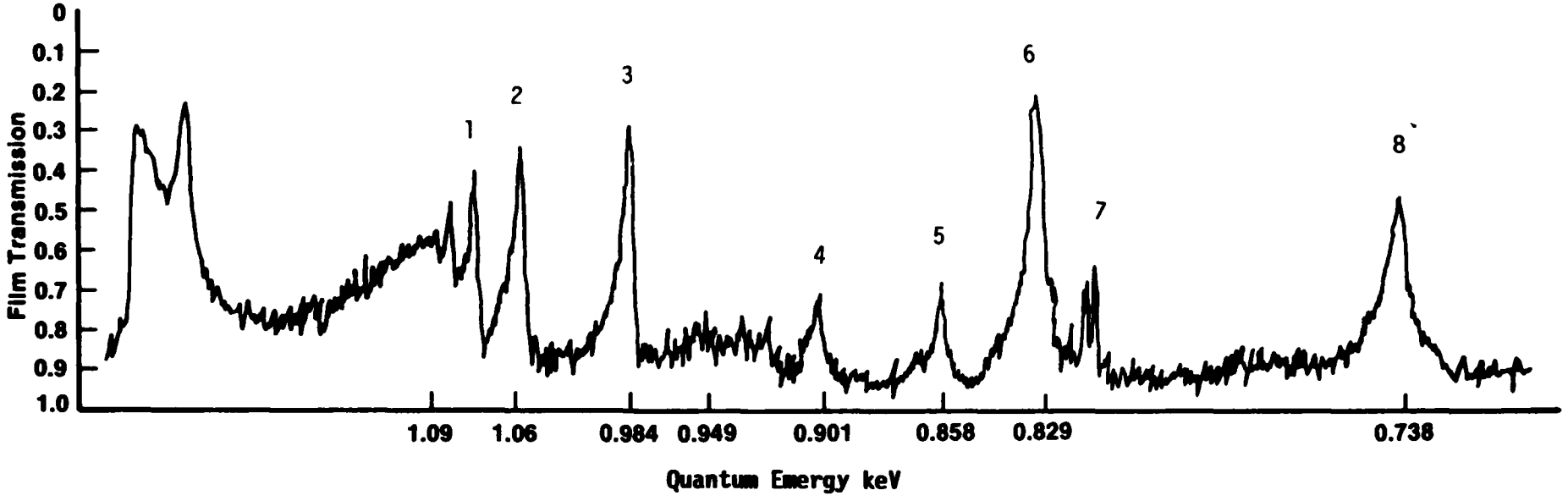

FIGURE 6. DENSITOMETER TRACE OF F X-RAY SPECTRUM

Single shot ∿100J laser pulses were used for absorption studies to give larger plasmas (∿150 μm) and emphasize absorption. For the liine profile studies the x-rays were dispered by or flat KAP crystal and the x-ray spectrum was recorded on type M films. The resolution obtainable in these experiments was calculated to be leV. Any absorption depression in the line profile should have been resolved in these expeirments. None was seen. It is probable that the Doppler broadening associated with the time integrated measurement through an expanding plasma with changing velocity smeared out the line profiles.

The L-line emitters are of greater significance as x-ray source for lithography of printed circuits. The L-line emitters which were studied include Cu, Fe, Cr, Ti, V, and Nb. The Ti and Nb represent the approximate upper and lower ends of the L-band of lines. With Ti, the strongest L-resonances lines are about 1/2 keV and very little L-line energy is above 1 keV. With Nb, the strongest resonance lines are at almost 2 keV, and are an order of magnitude weaker than the strongest resonance lines of Fe. In general we can see that ∿Cu will be the most efficient target for L-line radiation in the 1-1.5 keV energy band. Actually, the L-band for Cu starts with the large resonance lines at 0.95 and 0.98 keV. Probably Zn or Ga would be a little better in this energy band, but the surfaces are less suitable as laser targets and probably allow more depopulation of the amplifier by back reflection. Nd is an example of an element whose lowest lying L-resonance line of 1.86 keV is so high in energy that it is only weakly excited. (Figures 7, 8, and 10)

The M-line peak is of only marginal interest for x-ray lithography because it is an efficient producer only of very soft x-rays, on the order of a few hundred eV. Those elements such as W, whose M-lines are of an energy high enough to be interesting, are far on the wing of the efficiency peak.

The initial focal area was varied over a range of about an order of magnitude by changing the position of the target in the focal cone. These experiments were performed only with the Cu target, and the results are shown in Figure 9. Within the range of parameters evaluated, the change in focal area had almost the same effect on efficiency as the change in power density at a fixed focal area. This would indicate that most of the

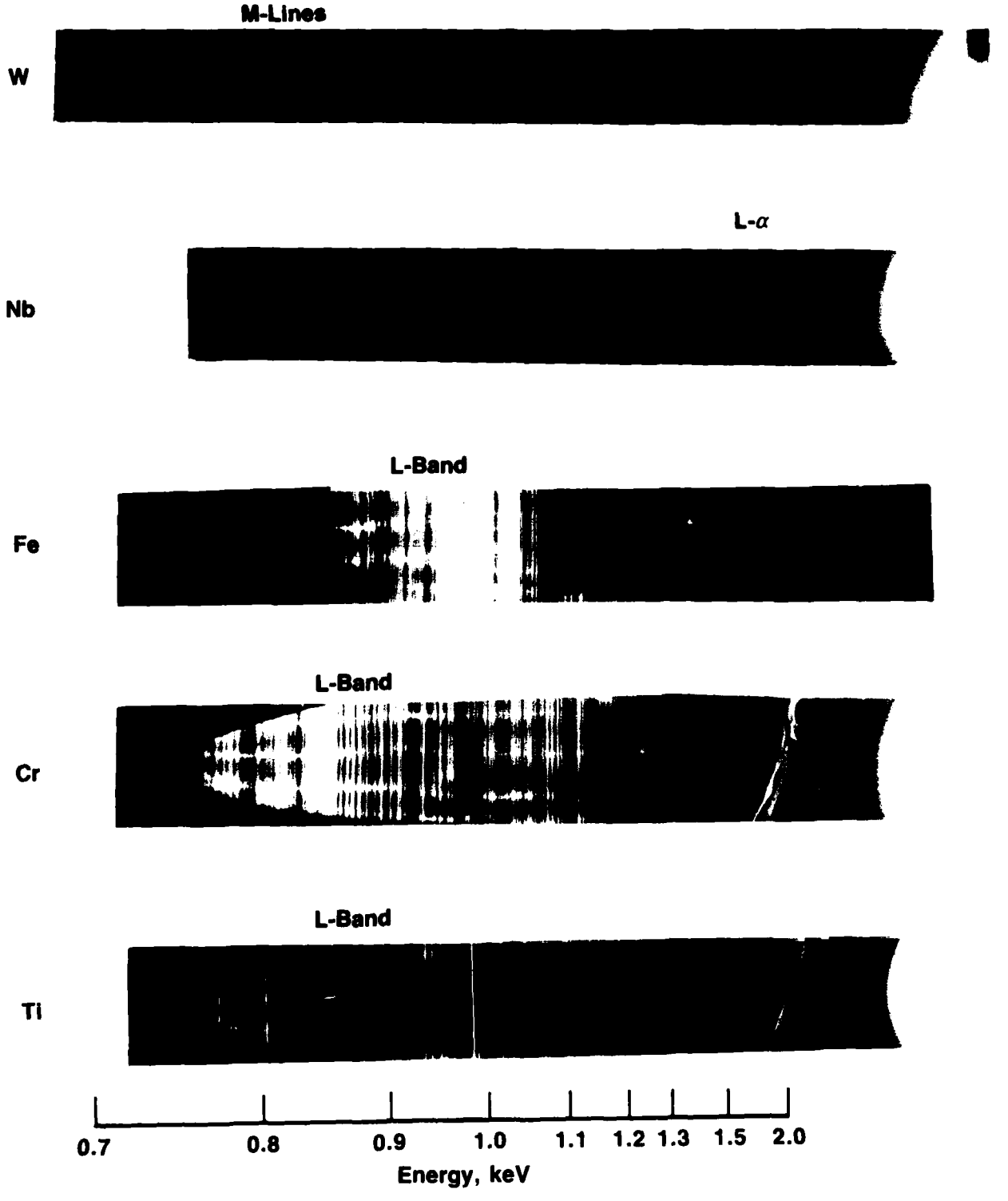

FIGURE 7. L AND M-LINE SPECTRA

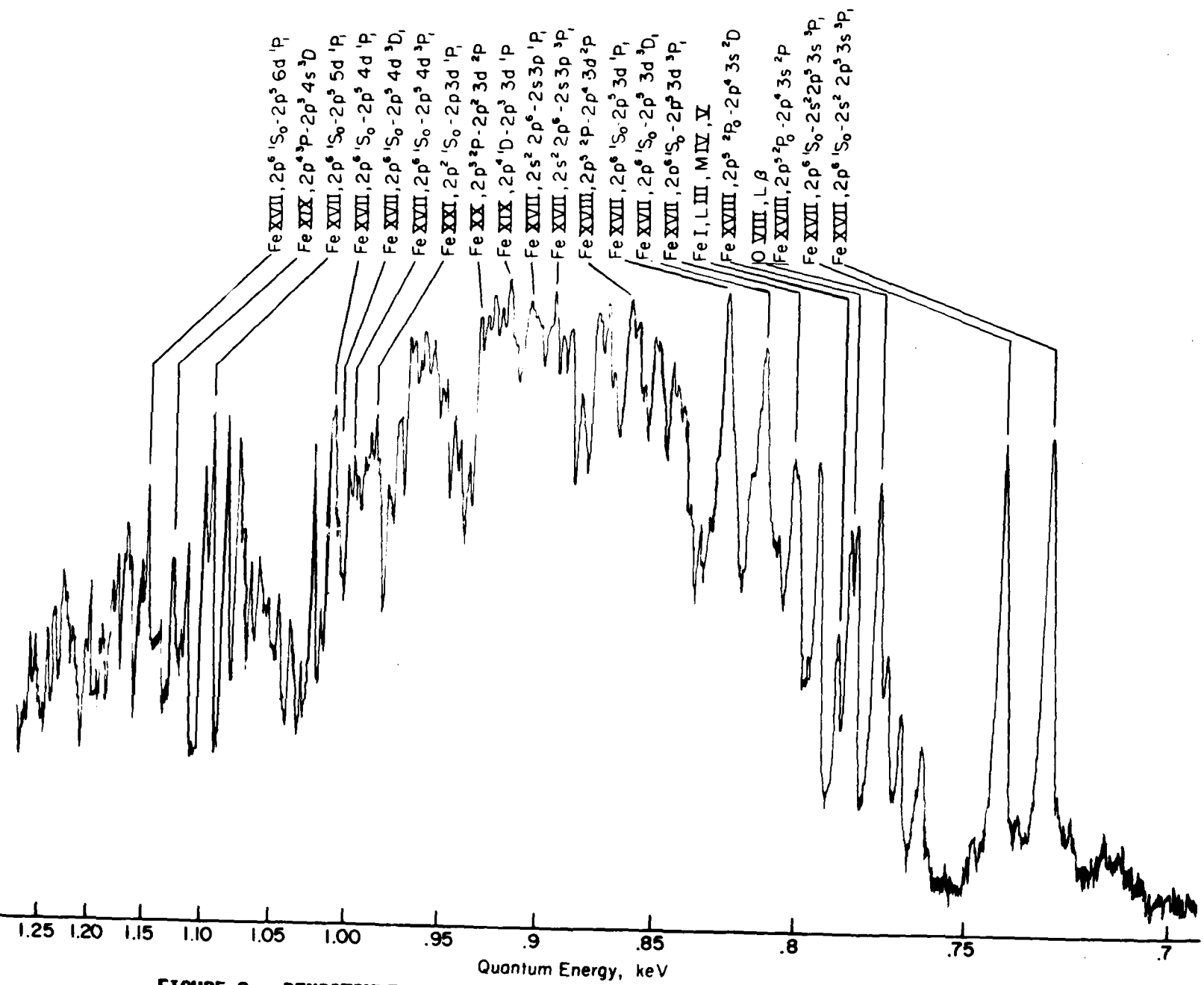

FIGURE 8. DENSITOMETER TRACING OF SPECTROGRAPH OF X-RAYS FROM IRON SLAB TARGET USING BENT CRYSTAL SPECTROMETER
(Laser flux is incident on iron slab at $\sim 10^{14}$ watts/cm^2)

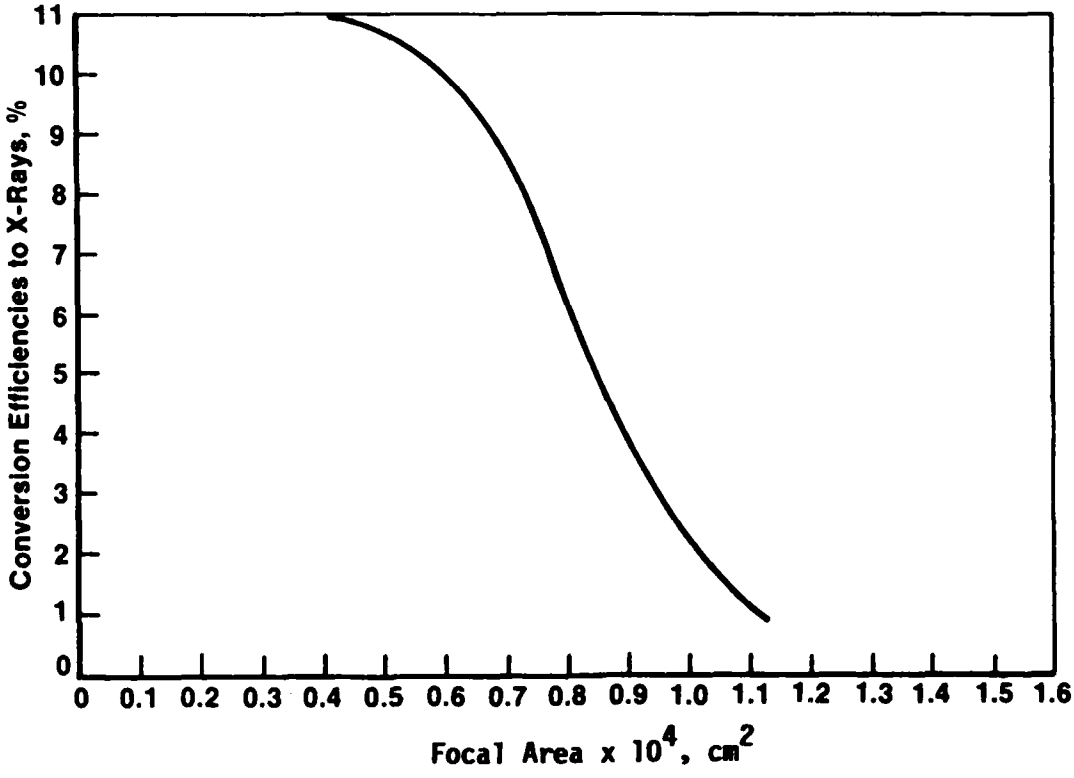

FIGURE 9. EFFECT OF FOCAL AREA ON X-RAY EFFICIENCY FOR 300 mj, 0.18 msec LASER PULSES

radiation is emitted while the geometry is still essentially planar. As shown in the computer printout of Figure 15, the critical density plane has moved only about 10 μm in 135 psec. This motion is small compared with the diameter of the focal spot.

Only two focal ratios were used in these experiments, f/13 and f/4.5. With the f/4.5 lens, the focal spot diameter was determined by the quality of the lens instead of the quality of the beam. The focal spot diameter for the f/13 lens was ∿100 μm. For the f/4.5 lens, the focal diameter was ∿70 μm. The conversion efficiency for the f/4.5 lens is approximately 1.5 times that for the f/13 lens in tests with 0.3j laser pulse of 180 psec pulse width. The optimum f number[6] is given by

$$f_{opt} = \left(\frac{v\,\tau}{D_B\,\Delta}\right)^{1/2}$$

Thus, the optimum f number for this system would have been ∿f/1, and it is expected that the smaller f number lens yields better conversion efficiency. If the laser were diffraction limited, the optimum f number would increase to 3.3 and the f/4.5 lens would be much better matched.

RESULTS OF PREVIOUS WORK

This section discusses the research performed at Battelle in the first years of this program and briefly discusses results of previous Battelle programs directed toward developing and evaluating the capability of the laser x-ray source for the x-ray lithography application.

Scaling Criteria

For the high-average power applications, it is advantageous to use a low pulse energy, high repetition rate laser. The high conversion rates of laser energy to x-rays (up to 27 percent over 300 eV) at Battelle have been achieved in tne near steady-state coronal plasma radiation regime with carefully pre-conditioned plasma profiles. The rule of thumb dividing line between steady state and time dependent coronal plasmas is given by $t \approx 10^{12}/n_e$. Since the critical plasma density where the principal absorption occurs is

$n_e \simeq 10^{21}$, radiation times greater than 1 nanosecond can be reasonably assumed to be steady state, if the plasma remains in the dense region for 1 nanosecond. This is an important factor if we are to assume, for scaling purposes, that the radiated x-ray spectrum depends only on the power density and electron density gradient at the critical-density surface. If quasi-steady state conditions have not been achieved, the spectrum will depend on previous irradiation history.

The focal diameter, D_f, at the critical surface of the plasma changes as the plasma moves out at a velocity v. If the laser is focused on the critical density surface at time t, D_f is given by

$$D_f = f\, D_B \Delta + v|t|f \tag{8}$$

where f is the f number of a perfect lens, D_B is the incoming beam diameter, Δ is the natural beam divergence, and v is the plasma velocity. The first term represents the initial focal diameter on the critical surface and the second is the increase in diameter due to the expanding plasma. The situation in which the laser is focused at the position which the critical density surface will occupy when the laser reaches peak power corresponds to t = 0 when the laser power is at its maximum. However, for purposes of scaling, this is not a factor.

The power density at focus, P, is given by

$$P = 4/\pi[f^2 D_B{}^2 \Delta^2/P_L + 2v|t|D_B\Delta/P_L + v^2t^2/(f^2P_L)]^{-1} \tag{9}$$

where P_L is the laser pulse power. In the steady state, v is a function only of P for a given target. If f and Δ are kept constant and t and D_B are scaled as $P_L{}^{1/2}$, P will remain unaffected. Thus, the spectrum and conversion efficiency will be conserved with this scaling. This type of scaling has been tested at Battelle over a laser pulse energy range of over 100, and found to be valid.

The optimum f number for the lens is given by

$$f_{opt} = \left(\frac{vt}{D_B\Delta}\right)^{1/2} \tag{10}$$

Of course, the f number of the lens cannot change with time on a nanosecond time scale. For a high average power system we would like to have P exceed a threshold for an extended time rather than have the peak power coincide with the minimum focal diameter. This also keeps v relatively constant through a large part of the pulse. Plasma velocity is a weak function of P anyway. Choosing the lens to optimize the power at time τ gives

$$P \simeq \frac{P_L}{\pi v \tau D_B \Delta} \tag{11}$$

In scaling, τ is proportional to the pulsewidth.

If high conversion efficiency is desired for low energy pulses, a short pulse width is required. However, it is not obvious why low energy pulses are desirable for a high average power laser source. Large pulse, solid state lasers are almost universally made of glass. Because of the thermal expansion and low pumping efficiency of glass, it is several times more expensive to obtain the same average power from a glass system than a YAG system. Unfortunately YAG rods are limited to small diameters (1 cm or less for commercial systems). It is, therefore, advantageous to be able to operate with low energy pulses. Since our past experience has shown that P should exceed $\sim 2 \times 10^{13}$ W/cm^2, a pulse energy under 1 joule requires a pulse width less than 1 nanosecond. Such pulse width can only be attained on commercial systems by mode locking. At this pulse width the $\sim$ 1 cm diameter YAG rod is limited to 0.3 - 0.4 joules per pulse if long life is required.

Experimental System

In typical x-ray lithography experiments, 100 joule light pulses with a nanosecond pulse width (full-width-half-maximum) were produced with a neodymium-doped-glass laser (1.06 μm wavelength) and focused onto flat copper targets to a spot size of 150 μm. Approximately 25 joules of x-rays were produced in the 0.3 to several keV regime on each shot. Of the 25 joules, approximately 10 joules were produced between 3/4 and 2 keV, which is the regime of greatest interest for high accuracy LSI production. A mask/wafer assembly was placed 10 to 20 cm away from the source. The x-ray outputs which are cited refer to x-rays radiated into the 2 π steradians facing the mask/wafer assembly.

The Laser

The laser used in prior research is a neodymium-doped-glass laser that delivers 1.06 μm-wavelength light pulses and consists of an oscillator (located at the far end of the room) followed by six amplifier stages arranged in series. The final stage contains a glass rod 64-mm in diameter. The capability of this equipment ranges from 100 joules in 1-1/2 nanoseconds up to 450 joules in 30 nanoseconds. X-ray optimization experiments were performed with this laser at a variety of laser energies and pulse widths. However, most of the actual wafer irradiations were performed with 100 joules of laser energy delivered in 3 or 4 nanoseconds.[6] A paper discussing the optimization of the laser and system for x-ray lithography is included as an appendix.[7]

The physical mechanism that converts the laser light into x-rays may be of interest. Briefly, the leading edge of the focused laser pulse vaporizes and ionizes the surface of the target and creates a low temperature plasma. The plasma that is created absorbs the remainder of the laser pulse by the inverse bremsstrahlung absorption process and is heated to a temperature of approximatley 1 keV (1.2×10^7 °K). X-rays are produced in this high temperature plasma by bremsstrahlung, recombination radiation, and line radiation, all of which originate from electron-ion collisions. For copper targets, the strongest x-ray component is line radiation.[6] (Figure 10)

Since the plasmas are usually not in a steady state and since the plasma electron temperature varies in both space and time, some discussion of the plasma temperatures derived from x-ray measurements is in order. Any determination of temperature by comparisons of ratios of lines from different ionization states is very questionable. Temperature determinations from the intensity ratio of satellite to resonance lines in the same ionization state are more justifiable. Satellites of the He- and H-like ions have been evaluated for several elements.[8,9] The temperature results from the H-like measurements should be acceptable in the time dependent corona regime because the populations in the upper level are produced dominantly by dielectronic recombination. (In the excitation of the He-like satellites, excitation from the inner shell of the corresponding Li-like ions plays a major role.)[8]

The temperature is most often derived from the measured shape of the continuum radiation. That radiation can be of two types: plasma bremsstrahlung, E_{ff} and recombination radiation, E_{fb}

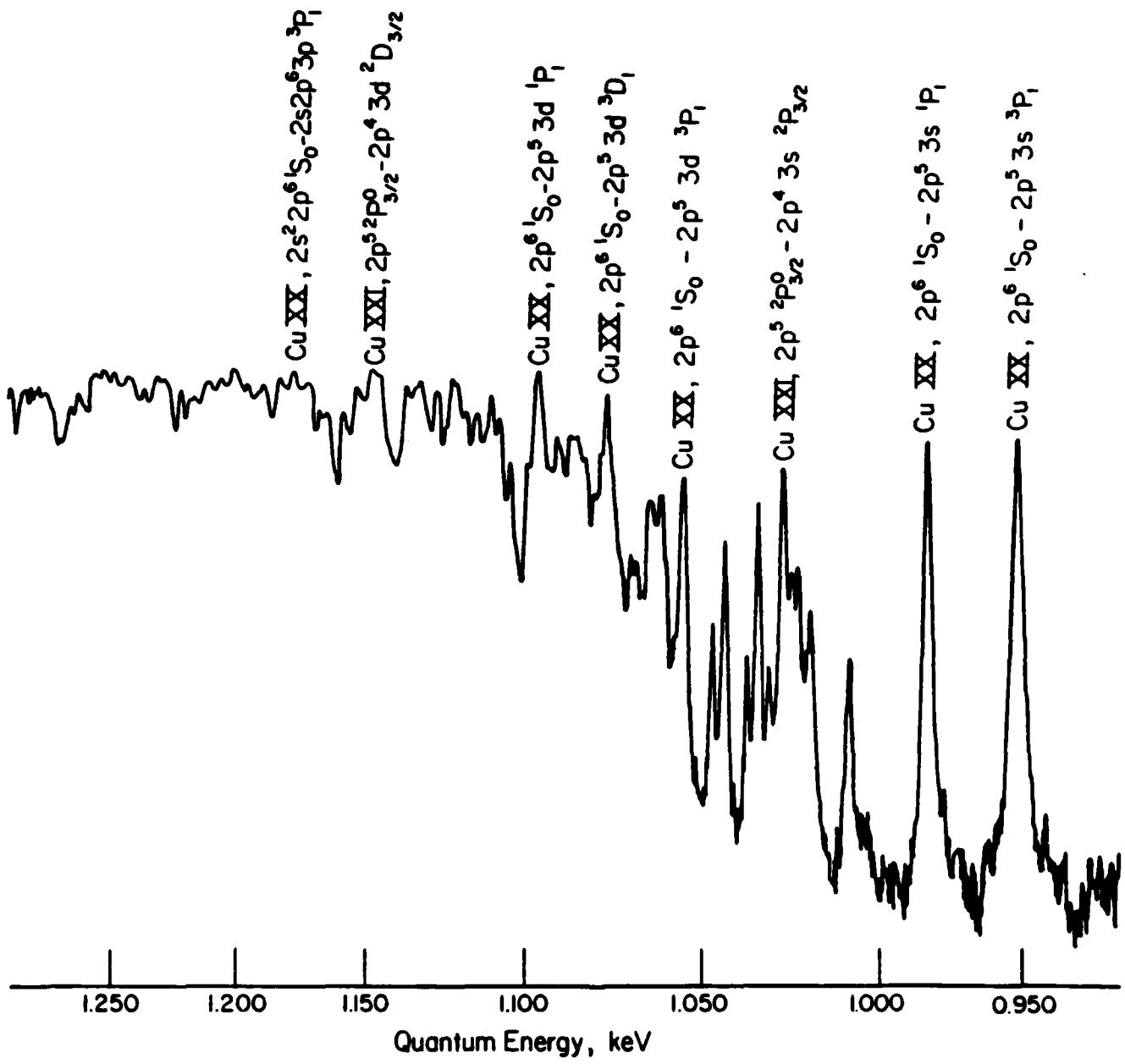

FIGURE 10. DENSITOMETER TRACING OF BENT CRYSTAL SPECTROGRAPH OF X-RAYS PRODUCED FROM COPPER TARGET WITH NEODYMIUM LASER PULSE

$$\frac{dE_{ff}}{d\nu} \sim \Sigma\, n_e n_i\, Z_i^2\, \frac{\exp(h\nu/kT_e)}{(kT_e)^{1/2}} \tag{12}$$

$$\frac{dE_{fb}}{d\nu} \sim n_e\, n_{i+1}\, Z_i^4\, \frac{\exp[-h\nu - \chi_{i,n})/kT_e]}{(kT_e)^{3/2}} \tag{13}$$

Because of the Z^4 dependence in the recombination radiation, this type of continuum will dominate for low kT_e. In fact, the plasma bremsstrahlung radiation will not equal the recombination radiation until

$$kT_e > 3\chi_H Z^2 \tag{14}$$

where χ_H is the energy of the hydrogen-like state.

The temperature can be directly derived from differential absorption measurement by evaluating the integral

$$\frac{I}{I_o} = \int_{\chi_i}^{\infty} \exp\,(\chi_i - h\nu)/kT_e \exp[-\Sigma(h\nu t)]\, d\,(h\nu) \tag{15}$$

where $\frac{I}{I_o}$ is the attenuation through a foil of thickness, t, and mass absorption cross section, $\Sigma(h\nu)$. For Be, in this range of interest

$$\Sigma(h\nu) \sim 570(h\nu)^{-3} \tag{16}$$

where $(h\nu)$ is in keV.

The principal x-ray emissions in the Al target experiments were He-like K lines and recombination radiation (Figure 11). Figure 3 shows the transmitted intensities as a function of Be absorber thickness for Al targets irradiated with 0.53 μm and 1.06 μm laser pulse 1.5 nanosecond in width. It can be seen that for low intensities the x-ray intensity is dominated by the He-like Al line (the $1S^2$ - 1S3 p transitions including satellites). As the intensity increases, the H-like Al line (1S3 p transition including satellites) becomes noticeable but not dominant. Finally at powers exceeding 5×10^{13} with the .53 μm wavelength, the recombination radiation becomes dominant. The plasma

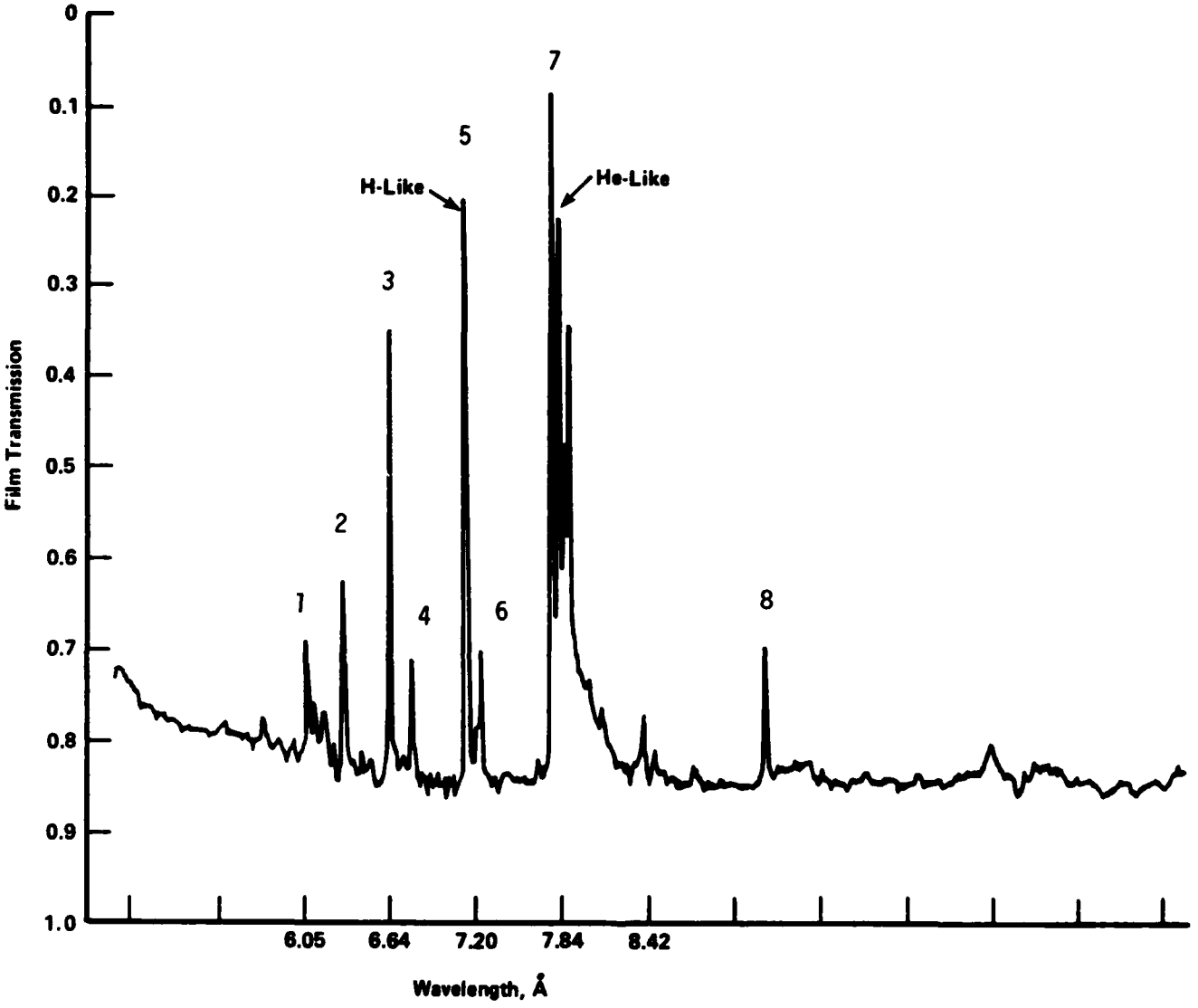

FIGURE 11. DENSITOMETER TRACE OF Al X-RAY SPECTRUM

electron temperature as determined from the slope of the absorption curve in the recombination regime is very weakly dependent on wavelength and is $\sim$ 600 eV for both the 1.06 and .53 μm wavelengths at 5×10^{13} w/cm^2.

Several interesting aspects of the laser-plasma phenomonology are evident from Figure 12. The Al targets irradiated with 1.06 μm laser light emitted dominantly He-like line radiation with recombination radiation representing a few percent of the total. This is true even at power densities of 10^{14} w/cm^2. However, the Al target irradiated with 0.53 μm laser light showed almost as much H-like as He-like Al emissions and the percentage of recombination radiation was about double the intensity for the same power level as the 1.06 μm tests. When the power is increased to $\sim 8 \times 10^{13}$ w/cm^2, the radiation is almost complete recombination. The temperatures, as determined from the slope of the absorption curve after subtracting out the contribution from the line radiation, are 600 eV and are essentially independent of the wavelength. Only a slight dependence of temperature on intensity is observed in the $4 - 8 \times 10^{13}$ w/cm^2 intensity range.

The intensities of the lines are of particular interest. Since the radiation temperatures are almost the same, we expect the line intensities to be proportional to $n_e n_{i,j} V$, where n_e is the electron density and $n_{i,j}$ is the density of ions in ionization state j. At a given temperature, the effective radiation volume, V, would be expected to be strongly dependent only on focal spot size and pulse width because the relative expansion is closely related to the ion thermal velocity. For $\sim 4 \times 10^{13}$ w/cm^2 the intensity ratio of the line radiation at .53 μm to that at 1.06 μm is $\sim$ 11 indicating that the radiation in the .53 μm use takes place from a region of about four times the density. This general result is expected since the critical density is proportional to $n\nu^2$ (assuming that the H- and He-like transitions have approximately the same probability). The sharp drop in line emission with only a small change in temperature as the laser intensity changes from 8 to 4×10^{13} indicates that the radiating zone shifts to the less dense zone in front of the critical density region near the temperature peak.

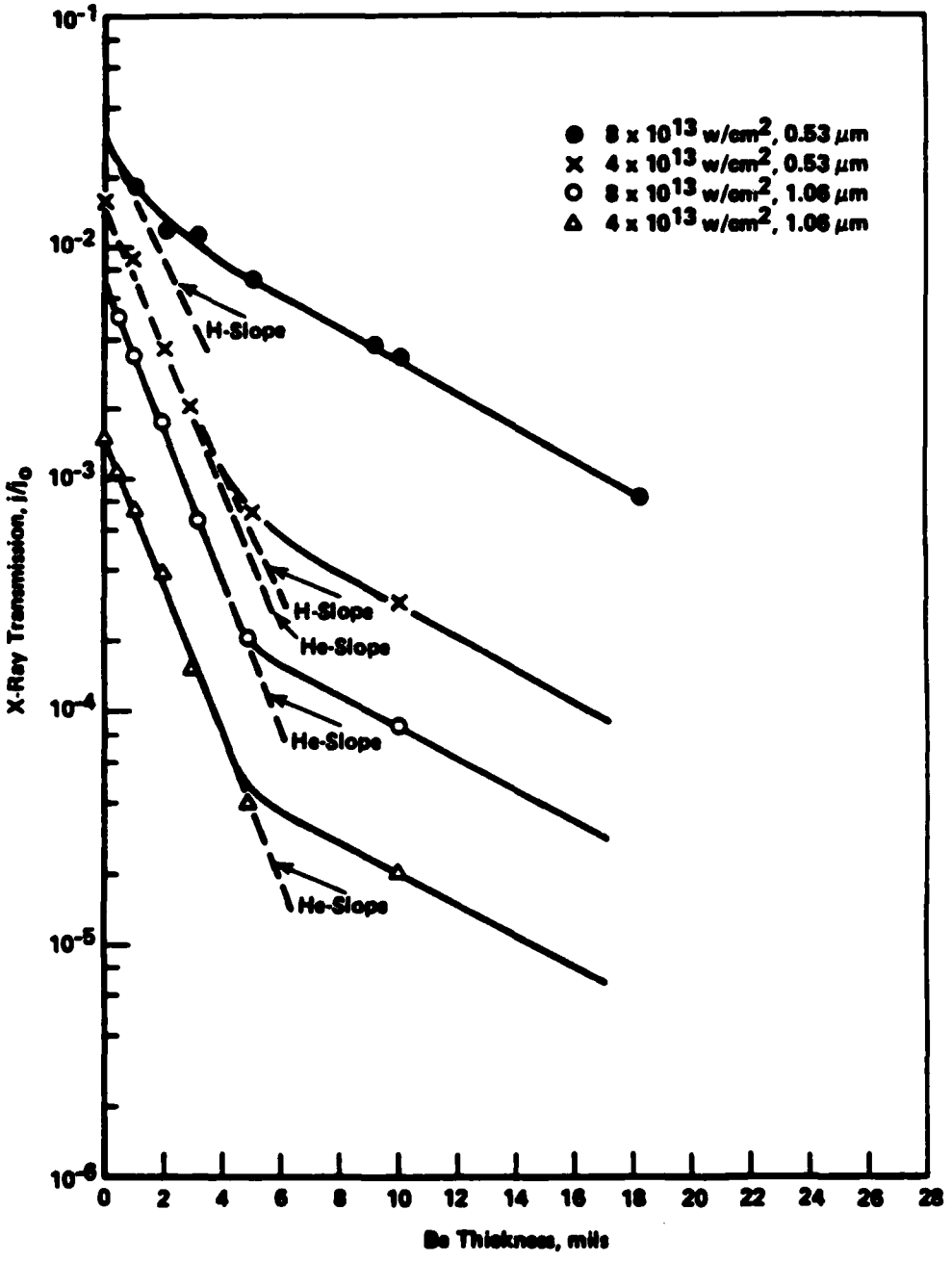

FIGURE 12. Al X-RAY TRANSMISSION THROUGH Be FOILS

Perhaps the most interesting observation from Figure 3 is the implied transition from a time dependent corona radiating plasma with 1.06 μm laser light incident to nearly steady state coronal plasma with 8×10^{13} w/cm^2 of 0.53 μm laser light incident. The steady-state ratio between consecutive ions in a corona model plasma may be represented by:

$$\frac{n(z,y)}{n(z+1,y)} = 7.87 \times 10^{-9} \chi(z,g)^2 \left(\frac{\chi(z,g)}{kT_e}\right)^{3/4} \exp\left(\frac{\chi(z,g)}{kT_e}\right) \qquad (17)$$

where $\chi(z,g)$ is the ionization potential of the ion of charge Z in its ground level g.

The temperature at which the population densities of the hydrogen-like state and the base nuclei are equal is shown in Figure 13.[10] At 600 eV the corona model predicts a ratio of H-like to He-like ions of ~ 0.25 and a ratio of completely stripped to H-like ions of ~ 0.2. This indicates that the plasma generated by the 1.06 μm laser pulse is not in coronal steady state. The 0.53 μm laser pulse at the 4×10^{13} w/cm^2 level appears close to the corona steady state. Since the relaxation time, τ, to the final state is given approximately by

$$\tau \sim 10^{12}/n_e \quad , \qquad (18)$$

it is not surprising that the higher density radiating regimes are closer to corona steady state. At the 8×10^{13} w/cm^2 level for 0.53 μm laser light the radiating plasma is stripped further than should be allowed by the temperature. This appears to show that the ions are stripped in a region of the plasma where the temperature is about 1 keV, but because of the lower transition rate for recombination radiation, the bulk of the radiation is emitted as the plasma expands and the electrons cool. Spatially resolved x-ray experiments are needed to confirm the phenomenology.

The L-line experiments with Cu targets are summarized in Figures 14, 15, and 16. Copper was already determined to be at the L peak of the conversion efficiency versus Z curve for x-rays above 1 keV and a power density of 10^{14} w/cm^2. It is not surprising that the radiation temperature is about 900 eV at 10^{14} w/cm^2 with 1.06 μm, because $e^{-\chi_{ij}/kT}$ is very nearly one for most

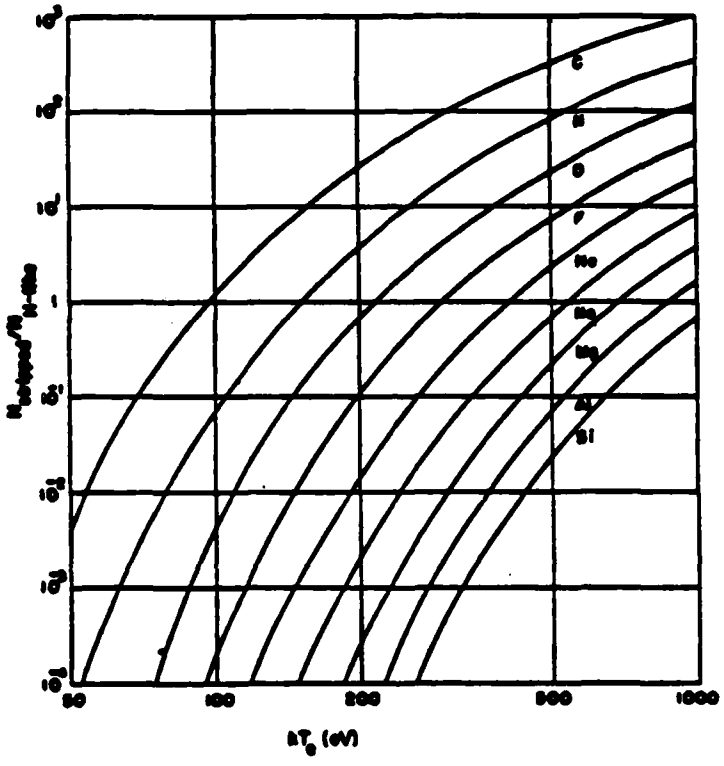

FIGURE 13. PREDICTIONS OF THE CORONAL EQUATION FOR THE RELATIVE POPULATIONS OF THE COMPLETELY STRIPPED ION TO THE HYDROGENLIKE ION AS FUNCTION OF dT_e

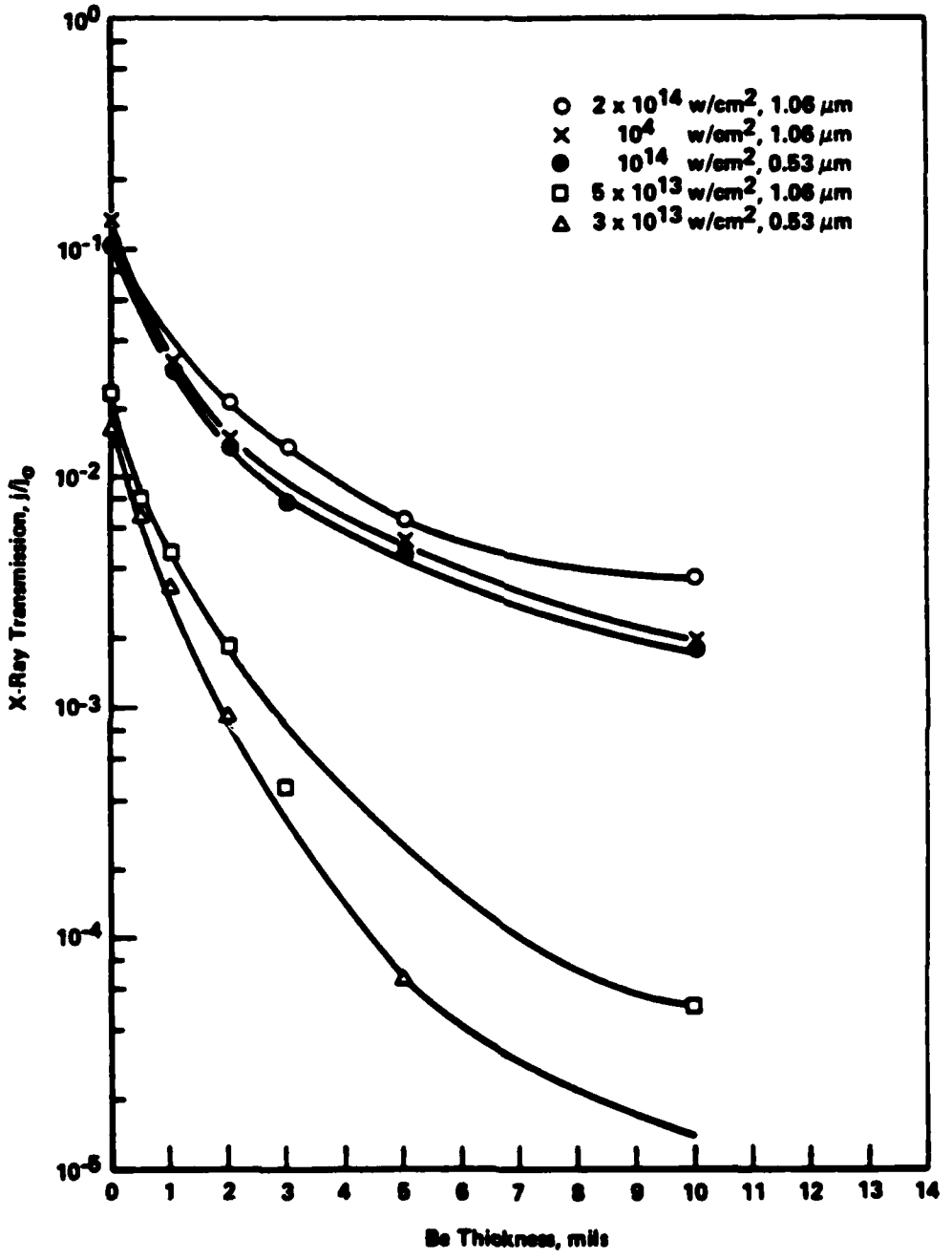

FIGURE 14. Cu X-RAY TRANSMISSION THROUGH Be FOILS

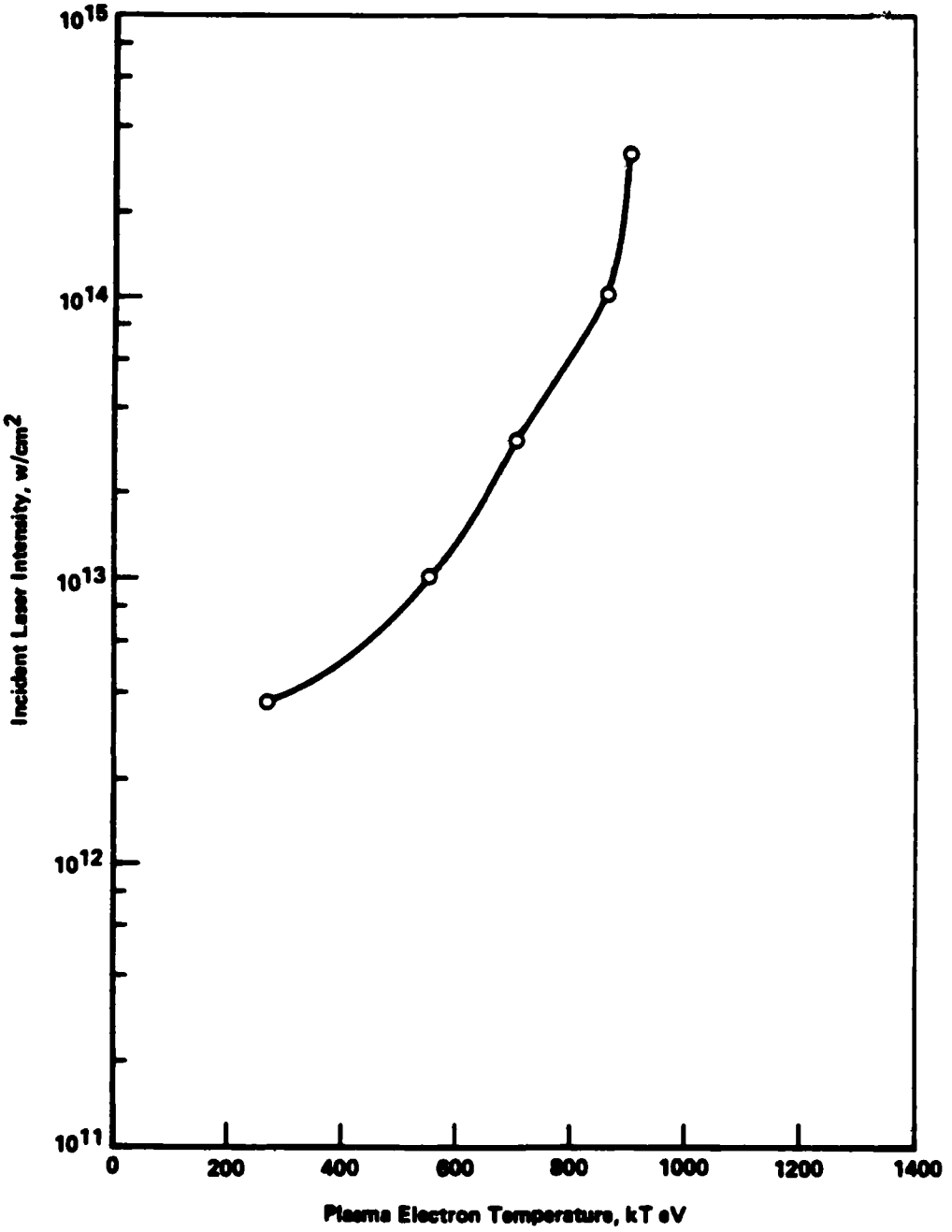

FIGURE 15. RADIATING PLASMA TEMPERATURE VERSUS INCIDENT LASER INTENSITY FOR Cu TARGETS

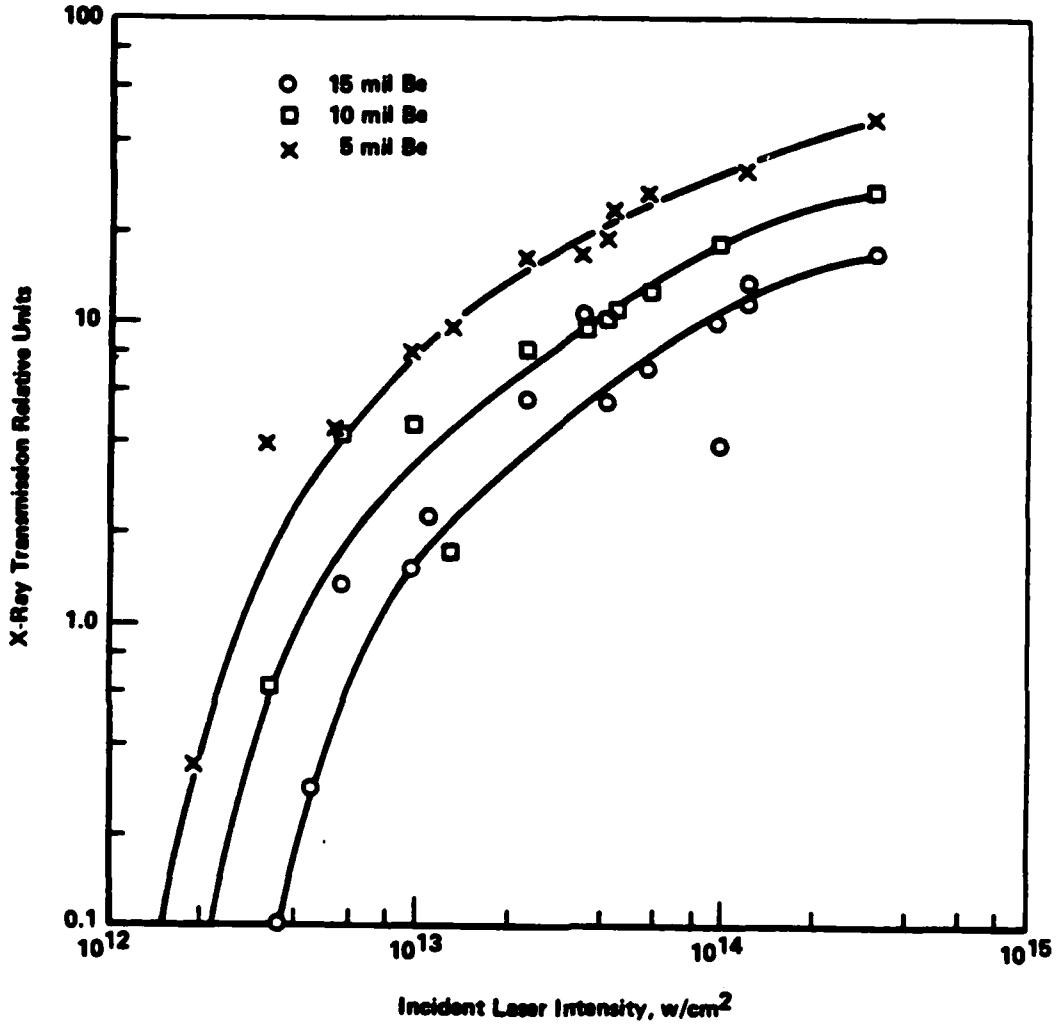

FIGURE 16. Cu X-RAY TRANSMISSION THROUGH THICK Be FOILS FOR 1.06 μm LASER PULSES

of the L line transitions. The 900 eV temperature would cause 80 percent of the Li-like ions to be stripped to the He-like states in corona steady state. This is again a demonstration that the ions have not reached steady state. (Figure 17) In the case of the 0.53 μm laser light, the situation is more complicated. The emitted radiation in the 10^{13} w/cm^2 incident laser light range appears to be essentially independent of incident wavelength. It is not surprising that the effective radiating temperature is about the same. Where there is an exponential dependence on temperature, the predominant radiation will tend to come from that region where the slope of the intensity variation with temperature begins to level. It is surprising that the conversion efficiency of laser light to x-rays is almost the same. This would suggest that the thermal conductivity is sufficiently high that temperature equilibration is more rapid than the ion state equipartition time, so that the exact location of the absorption does not appreciably affect the temperature or ionization state of the radiating regions. The one-dimensional "flash" calculations do <u>not</u> confirm this "quasi-isothermal" condition.

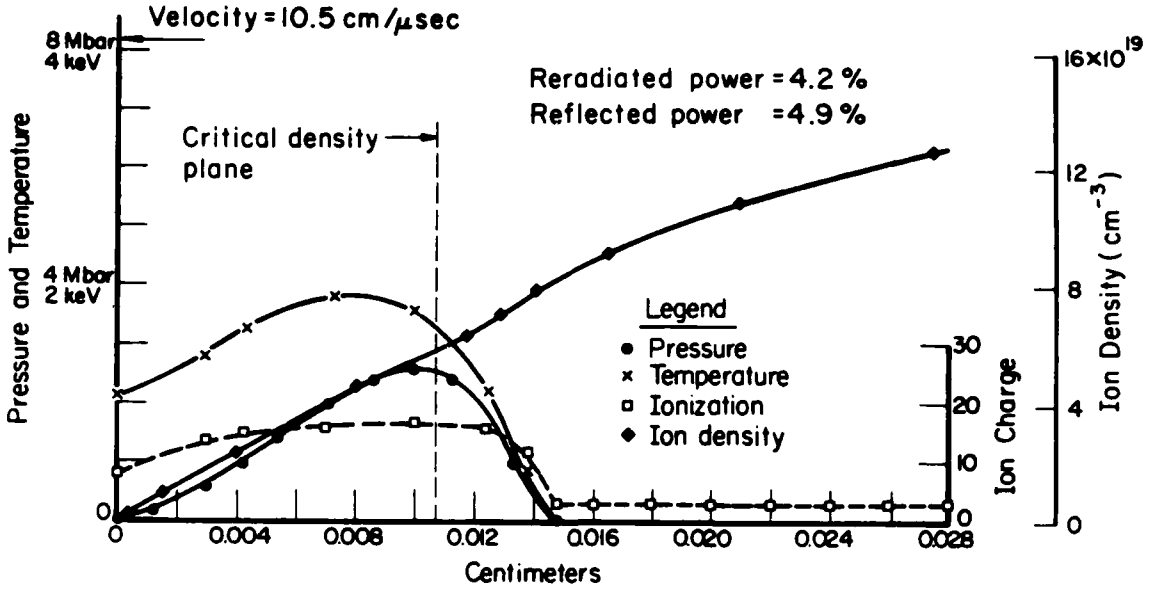

(a) Time = 33.4 Picoseconds

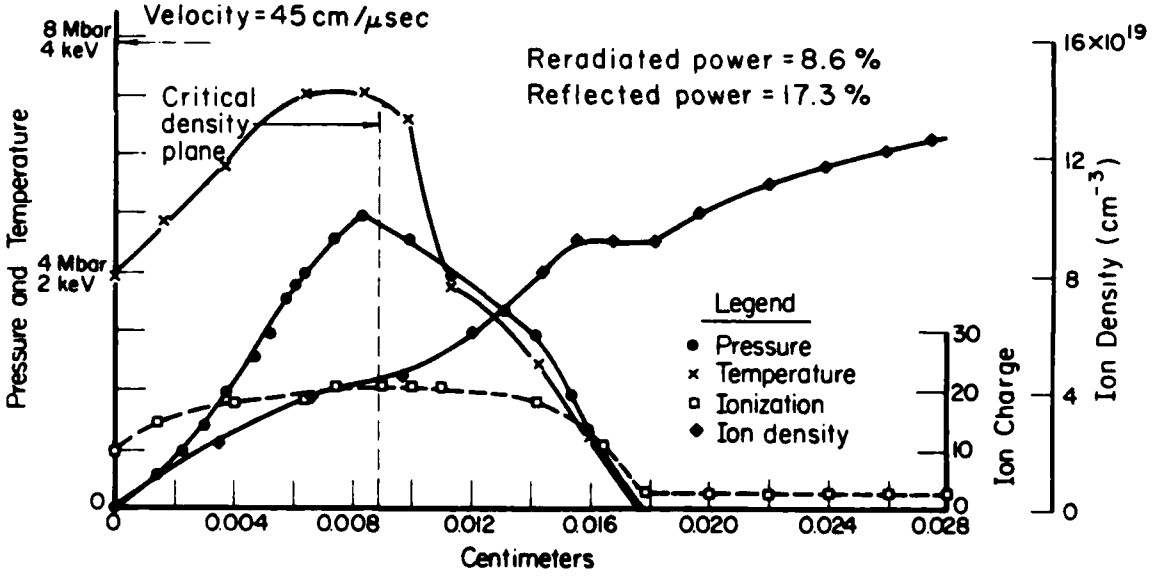

(b) Time = 86.8 Picoseconds

FIGURE 17. NONEQUILIBRIUM IRON CALCULATION: TIME-DEPENDENT IONIZATION

Incident laser flux = 1.05×10^{14} watts/cm^2
Wavelength = 1.06 microns

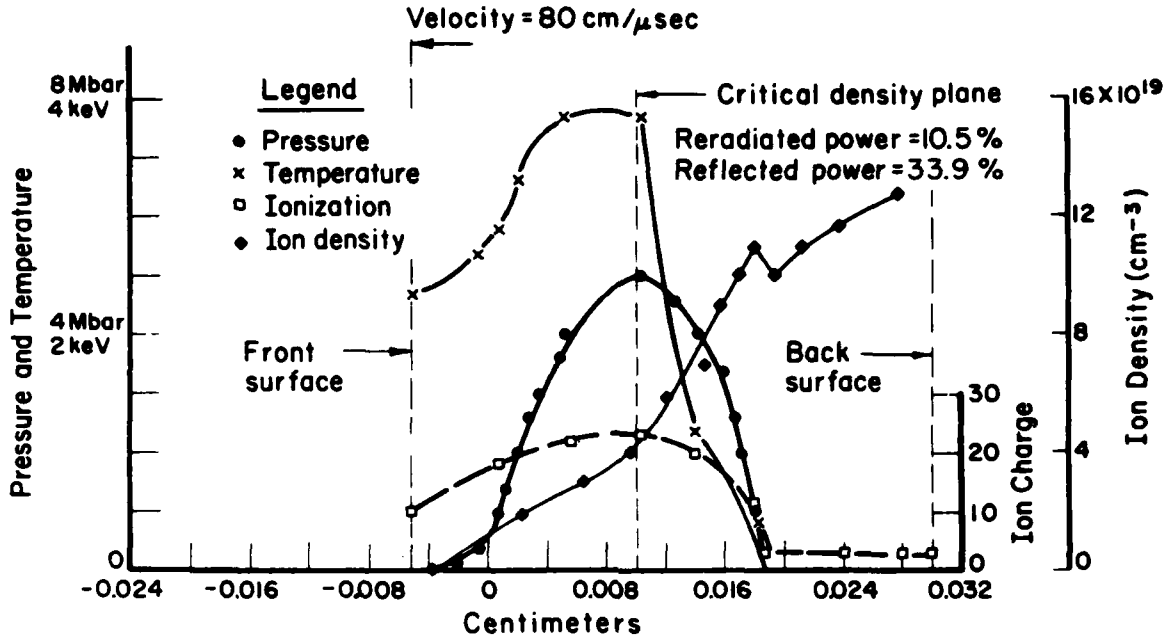

(c) Time = 135 Picoseconds

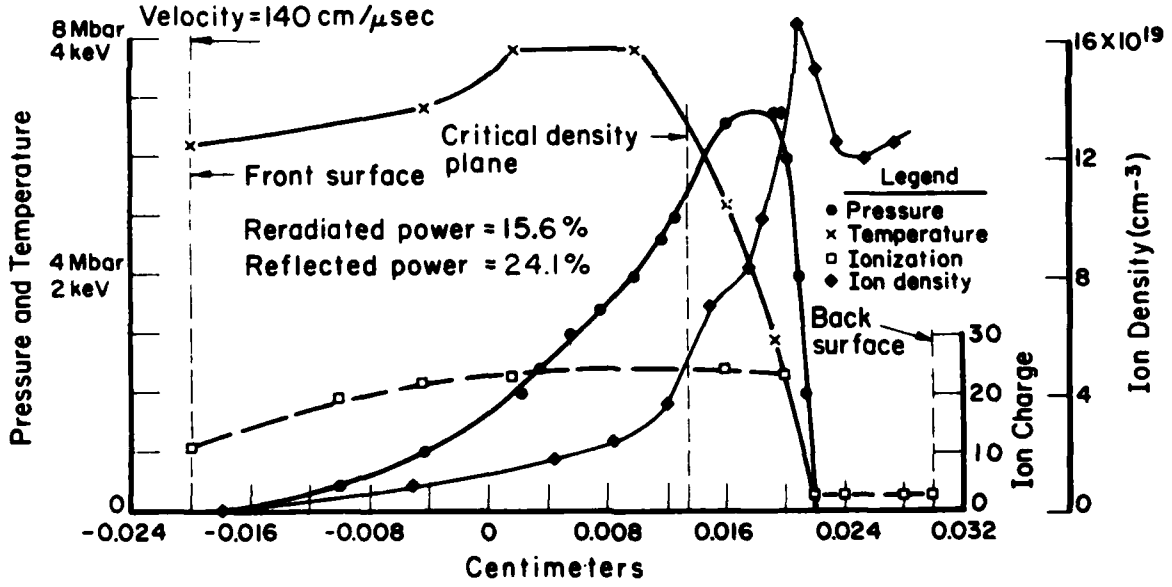

(d) Time = 265 Picoseconds

FIGURE 17. (Continued)

REFERENCES

(1) Smith, H. I., and Flanders, D. C., Japanese J. Appl. Phys., 16, Suppl. 16-1, 61-65 (1977).

(2) Nuttleman, R. H., Epstein, H. M., Beal, J. W., and Mallozzi, P. J., in Advances in x-RAY ANALYSIS, Eds. W. L. Pickles, C. S. Barrett, J. B. Newkirk, and C. O. Raad, 18, Plenum Press, New York (1975).

(3) Windsor, M. W., in Physics and Chemistry of the Organic Solid State", Eds. D. Fox, M. M. Lobes, and A. Weissberger, Vol. II, Interscience (1965).

(4) Laustriat, G., in Organic Scintillators", Ed. Horrocks, D. L., Gordon and Breach (1966).

(5) Dugay, M. A., and Olsen, J. N., IEEE J. Quant. Elect., 170-72 (April, 1979).

(6) Mallozzi, P. J., Epstein, H. M., Jung, R. G., Applebaum, D. C., Fairand, B. P., and Gallagher, W. J., "X-Ray Emission from Laser Generated Plasmas", Battelle Report on ARPA Contract DAAH01-71-C-0550 (February, 1972).

(7) Epstein, H. M., in Material Processing Symposium", Ed. Metzbower, E. A., ICALEO, LIA, Vol. 38 (1984).

(8) Boiko, V. A., Piluz, S. A., and Safronova, U. I., "The Analysis of Satellites to the H-Like Ion Resonance Lines Observed in the X-Ray Region, Mon. Not. R. Astr. Soc., 118, 107-120 (1978).

(9) Bhalla, C. P., Gabriel, A. H., and Presnyakov, L. P., Mon. Not. R. Astr. Soc., 172, 359 (1975).

(10) Stratton, T. F., Plasma Diagnostic Techniques, R. H. Huddlestine and S. L. Leonard, Eds., Chapter 8, Academic Press, New York (1965).

END

FILMED

10-85

DTIC